Investigation of the high-frequency wavefield of an off-center monopole acoustic logging-while-drilling tool

Hua Wang[1], Guo Tao[2], and Michael C. Fehler[3]

ABSTRACT

During logging-while-drilling (LWD) operations, complex drill string movements and the weight of the drill pipe often lead to a measurement tool that is not centralized. Therefore, studies of the response of an off-center acoustic LWD tool are essential to facilitate better interpretation of measurements made in an actual drilling environment. Such studies will be helpful for tool design and data processing. We used a finite-difference method to simulate the response of a noncentralized monopole acoustic LWD tool at high frequency (10 kHz). We analyzed the effects on the waveforms for receivers at different azimuths caused by an off-center tool with differing amounts of offset. We used velocity-time semblance and dispersion analysis methods to help us to understand the modes in the waveforms at different azimuth receivers for different tool offsets. We have found that the waveforms in the direction of the tool offset, that is, where the fluid column is smallest, were affected the most. Waveforms in the orthogonal direction were less affected by tool offset. Collar flexural and collar quadrupole modes appear when the tool is off center. In addition, the formation flexural and quadrupole modes contaminate the Stoneley wave. Waveforms in a fast formation are more strongly affected by the offset of the tool than those in a slow formation. In a fast formation, the new collar modes make it difficult to determine the P-wave velocity in the direction of tool offset whereas it is easier in the orthogonal direction. However, P-waves are less contaminated by new modes in a slow formation. Due to the significant changes in waveforms with azimuth when the tool is off center, the simple addition of all waveforms from an azimuthal distribution of receivers will not result in a clean waveform that is sensitive to only the surrounding formation.

INTRODUCTION

Acoustic logging while drilling (ALWD) is an advanced technology that is used in exploration geophysics and petroleum engineering to determine the elastic parameters of the formation during drilling. It is the only option for some special operations such as logging in a horizontal offshore well (e.g., Wang et al., 2009a). A great deal of research in ALWD leads to the conclusion that the velocities of the P- and S-waves can be reliably measured in fast formations by a tool with a monopole source. Successful measurements require that the effect of the drill collar on the waveforms are eliminated by some means (e.g., Leggett et al., 2001; Wang et al., 2009b; Kinoshita et al., 2010; Zhan et al., 2010). The effects of the drill collar on the processing and interpretation of ALWD data are

analyzed by Moore et al. (2008). In a slow formation, the P-wave velocity can be determined from the leaky-P when using a monopole tool (Tang et al., 2004; Wang and Tao, 2011). However, all of these conclusions are based on studies for the case in which the ALWD tool is centralized in the borehole. In field applications, the acoustic source and the receivers are embedded on the outer edge of the drill collar. The complex movements and the weight of the drill pipe lead to the tool being off center. Tang et al. (2009) analyze field data and find that a decentralized tool may have the same influence on Stoneley (ST) waves as a permeable formation. It is thus essential to better understand the response for an off-center tool because this case is closer to the field drilling environment. Knowledge about the effects of a tool being off center will be helpful for the design of new tools and in data processing. We

follow the terminology of the logging community and use the expression tool eccentricity to describe tool offset.

Studies on ALWD with an off-center LWD tool are rather limited. Wang and Tang (2003) evaluate the effects of an off-center quadrupole LWD tool on the simulated waveforms. They do not study the case of the tool being severely off center but conclude that data acquired using an off-center tool could be corrected. Tang et al. (2003) analyze a field data set from a quadrupole tool in a deviated well (30°–40°) and find that only a small-amplitude collar wave interfered with the high-amplitude quadrupole wave. Huang (2003) finds that a strong dipole mode was excited in the cases of off-center monopole and quadrupole tools with a low frequency source (2 kHz) in a slow formation. Huang et al. (2004) and Zheng et al. (2004) analyze the effects of tool eccentricity on wavefield dispersion characteristics. All of these studies indicate that there are two main effects of the tool eccentricity on waveforms. First, more modes are excited, which will lower the amplitude of the symmetric modes. For example, the ST wave will appear in measurements made with off-center dipole and quadrupole LWD tools. Second, the tool eccentricity influences the dispersion of the modes. The ST wave will be weakly dispersive, and dipole and quadrupole modes will be split. Wang et al. (2013a) study the wavefield of an eccentric multipole ALWD tool in a slow formation and propose a method to quantify the eccentricity of the tool.

The above studies are mainly focused on the responses of off-center dipole and quadrupole LWD tools. However, monopole tools are widely used to acquire the P-wave in fast and slow formations. As a result, the study of an off-center monopole tool is of the same importance as that of dipole and quadrupole tools. Only Huang (2003) and Wang et al. (2013a) study the response of an off-center monopole tool. Huang (2003) studies the wavefield of the off-center monopole tool with the extent of eccentricity of 10.95 mm in a 234-mm-diameter wellbore at a low frequency (2 kHz). She finds that a strong dipole mode appears on the receiver in the direction of the tool eccentricity (i.e., the direction of least spacing between the eccentric tool and the borehole); the monopole mode in the orthogonal direction is not affected. The off-center monopole tool does not severely affect the determination of the velocity of P-wave. Her study only considers slow formations and low-frequency monopole sources. Wang et al. (2013a) also study the response of an eccentric monopole tool at low frequency (2 kHz) in a slow formation. The monopole source can also be operated at frequencies as high as 10 kHz or more. Pardo et al. (2013) use a finite-element method (FEM) to study the responses of the eccentric monopole tools in fast and slow formations for wireline and LWD cases. However, they only study the waveforms at one azimuth and one tool offset. Therefore, it is necessary to further study the wavefield for a high-frequency off-center LWD monopole tool in fast and slow formations and at different azimuths and different tool offsets.

Realistic numerical simulation on the wavefield of ALWD with the off-center tool requires that the sources and receivers to be exactly symmetrical about the tool. In our previous study (Wang et al., 2013a), we use a 3D FEM to simulate the wavefield rather than a staggered finite-difference method (FDM) (e.g., Wang et al., 2013b). FEM was shown to be reliable, but the computational cost is too high to allow a large number of simulations to be conducted. Considering the limitation on computation resources, we improved the staggered-grid FDM so that the point sources and receivers can be azimuthally distributed and exactly symmetrical about the center

of the tool. We validate the resulting FDM using a discrete wavenumber integration approach, which works well for the azimuthally symmetric case of a centralized tool. We will then study the response of the off-center monopole tool at high frequencies in fast and slow formations.

ACOUSTIC LOGGING-WHILE-DRILLING SIMULATION MODEL

We use a 3D FDM that has second-order accuracy in space and time to simulate the wavefield of the high-frequency (a Ricker wavelet with a central frequency of 10 kHz) off-center monopole tool in fast and slow formations. The complex frequency shifted perfectly matched layer method is used to eliminate the reflection from the truncated boundary of the simulation region (Wang et. al., 2013b). Figure 1 shows the model for the acoustic LWD simulation. Figure 1a gives a top-down view of the model. The formation outside the borehole is not shown. From outside to inside of the borehole, the media are the outer fluid, collar, and inner fluid. The acoustic sources are embedded on the outer edge of the drill collar. A total of 36 point sources are used to simulate the response of the ring source in the real logging operation. A total of 36 point receivers are also located around the collar for each receiver offset (8 offsets used). The side view of the model is shown in Figure 1b. Formation and borehole media properties are given in Table 1. The radius of the borehole is 117 mm, and the inner and outer radii of the collar are 27 and 90 mm, respectively. The dimensions of the simulation model are 0.6, 0.6, and 4.55 m in x, y, and z, respectively. The source is located at $z = 0.45$ m and the receivers at eight different offsets are located from $z = 3$ m to $z = 4.05$ m with a minimum source-receiver spacing of 2.55 m and receiver offset separation of 0.15 m along the borehole. We used a 3-mm grid in the FDM. The next section discusses the reliability of the FD simulation.

During our discussion, we will only consider the distance between the center of the tool and the borehole center. We will not change the angle of the tool relative to the borehole. We will shift the entire tool an equal amount toward the edge of the borehole.

VALIDATION OF THE FINITE DIFFERENCE CODE FOR A MONOPOLE LWD TOOL

To check the validity of the FDM for the ALWD simulation, we compare the simulated waveforms for a centralized monopole LWD
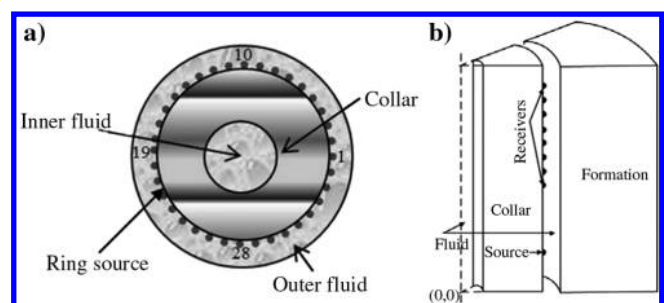

Figure 1. The model for the ALWD simulation. (a) Top-down view of the model. Shown from outside to inside the borehole are the outer fluid, collar, and inner fluid. The formation outside the borehole is not shown. The acoustic sources are embedded on the outer edge of the drill collar, and the configuration of the 36 point sources of the ring source is shown. (b) Side view of the model.

tool obtained using two methods: (1) the FDM and (2) the discrete wavenumber integration method (DWM) (e.g., Wang and Tao, 2011). The waveforms obtained for fast and slow formations at receiver 1 for a 10-kHz source are shown in Figure 2a and 2d, respectively. The black solid and the gray dotted lines are the results from the DWM and FDM, respectively. The results obtained using the two methods are almost identical. The amplitude of the collar wave is very small, and therefore it is magnified for display. We can clearly see all the modes. For the fast formation, we see the collar, P-, S-, pseudo-Rayleigh (pR), and ST-waves. For the slow formation, we see the collar, leaky-P, and ST-waves. The arrival times and velocities can be found in the corresponding velocity-time semblance plot (Kimball and Marzetta, 1984): Figure 2b for the array

waveforms in Figure 2a and Figure 2e for the array waveforms in Figure 2d.

It is obvious that the collar wave and P-wave in the fast formation are well separated due to the choice of the formation velocities. It is difficult to separate the two modes for fast formations in which the velocity difference between the collar and formation is not large. Our choices for velocities were made to facilitate the detailed investigation of eccentricity of the monopole tool on the P- and collar waves. From Figure 2a and 2d, the waveforms from the FDM and DWM match very well. There is only very little difference in the ST wave, which is caused by numerical dispersion in the FDM.

To further investigate the waveforms, we use a method proposed by Dziewonski et al. (1969) to calculate the dispersion curves from

Table 1. Parameters for the borehole models.

	V_P (m/s)	V_S (m/s)	Density (g/cm^3)
Borehole fluid	1470	—	1.00
Collar	5860	3300	7.85
Outer fluid	1470	—	1.00
Fast formation	3000	1800	2.00
Slow formation	2000	1000	2.00

Note: V_P and V_S are the velocity of the P- and S-waves, respectively.
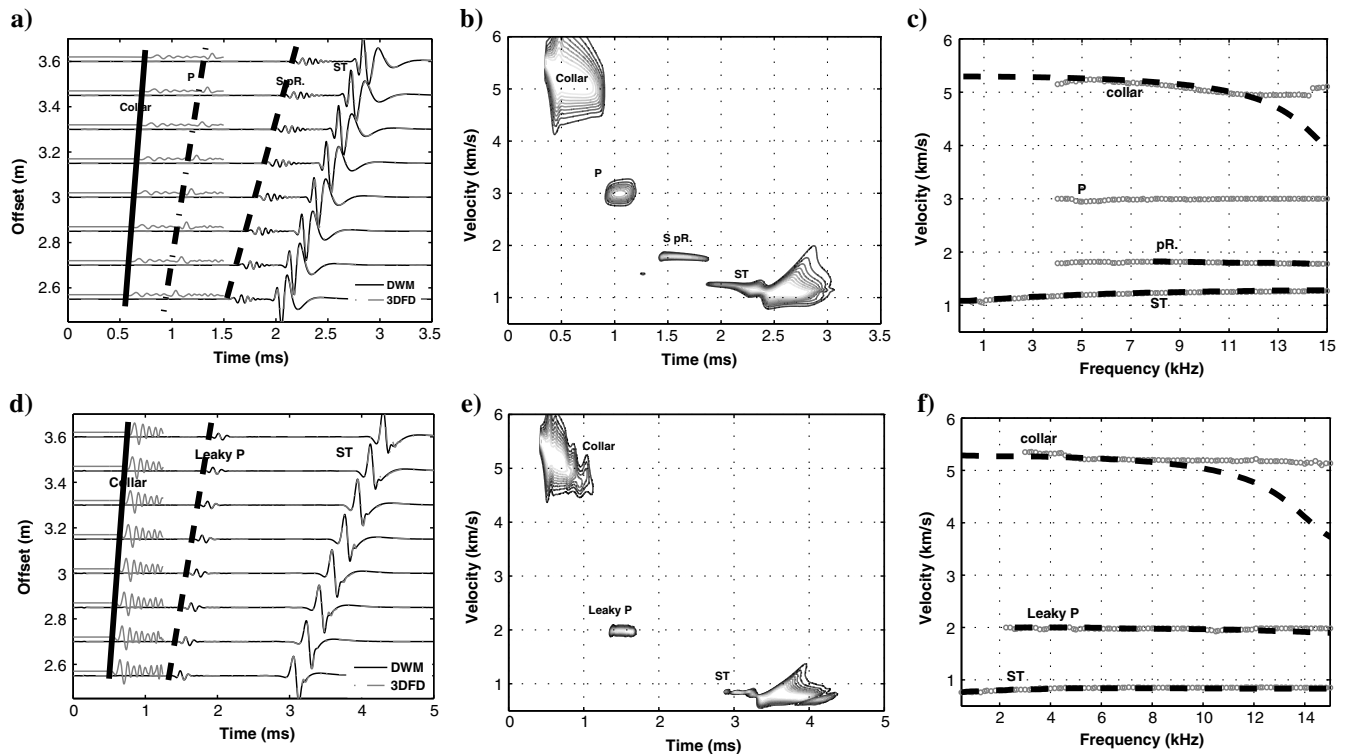

Figure 2. Benchmark waveforms for a centralized monopole LWD tool at 10 kHz in the fast formation calculated using FDM and DWM. Panels (a and d) are the waveforms for receiver 1 for the fast and slow formations, respectively. The black solid line and the gray dotted line are for the result from DWM and FDM, respectively. The small-amplitude collar waves are shown at the higher amplitude. Panels (b and e) are the velocity-time semblance plots for panels (a and d), respectively. Panels (c and f) are the dispersion analysis for panels (a and d), respectively. The modal dispersion curves are plotted as a dashed line. The calculated dispersion using array traces at all eight offsets are also shown as gray circles.

array waveforms. In this method, the choice of the number of filter bands must be made based on the desired frequency resolution and computational speed. Here we follow Rao and Toksoz (2005) by using Gaussian filters with a constant relative bandwidth to optimize the space-time resolution. The calculated dispersion using array traces at all eight offsets are shown as gray circles in Figure 2c (fast formation) and Figure 2f (slow formation). The modal dispersion curves are plotted as overlapping dashed lines in Figure 2c and Figure 2f. These curves are found by determining the solution of setting the determinant of matrix **M** equal to zero in equation 4 of Wang and Tao (2011) by using a root-finding Newton-Raphson mode-search routine (Tang and Cheng, 2004). The good agreement between the dispersion calculated from array waveforms generated by FDM and modal dispersion curves also illustrates the high accuracy of the results of FDM. The only minor differences between dispersion curves found by the two approaches are for the high-frequency band (above 10 kHz).

RESPONSE OF THE ECCENTRIC MONOPOLE ACOUSTIC LOGGING-WHILE-DRILLING TOOL IN A FAST FORMATION

Because making velocity measurements in a fast formation is a primary task, it is necessary to investigate the response of the eccentric monopole ALWD tool in a fast formation. We have used FDM to simulate the response of the monopole ALWD tool with different eccentricities in a fast formation, and the resulting waveforms from receivers at different azimuths are shown and discussed below. To analyze the details of the effect of eccentricities on different modes, we look into the relatively smaller collar wave and P-wave first. Then, we discuss the S- and ST-waves.

Figure 3 shows the collar and P-waves for receivers at different azimuths for different tool eccentricities. Polar coordinates are used to illustrate the waveforms from receivers at different azimuths. The circumference of the plots denotes the azimuth of receiver with respect to receiver 1, located in the direction of the tool offset, and the radial direction is time. Time goes from 0 to 1.5 ms. The waveform amplitude can be easily discerned. Figure 3 shows the waveforms for the tool eccentricities of 0, 3, 6, 9, 12, 15, and 18 mm. The same maximum-amplitude scale is used for all the waveforms, except that Figure 3f and 3g is minified five times.

From Figure 3, we can see that the arrival time of the collar wave for different amounts of tool eccentricity are approximately 0.5 ms and that the P-wave arrival times are approximately 1 ms. The eccentricities hardly change the arrival times of the collar wave. The amplitude of the collar wave fluctuates as eccentricity increases. Amplitudes become smaller as the fluid column becomes wider (near receiver 19, approximately 180° from the direction of tool offset). Figure 3h shows the collar waves at receiver 19 (azimuth angle of 180°) for different tool offsets. The amplitudes of the collar waves decrease with increasing tool eccentricity. For azimuths in which the column gets smaller (near receiver 1, approximately 0°), the amplitudes become larger as the tool eccentricity increases. Amplification of the collar wave is quite obvious when the fluid column size is reduced. However, the amplitudes hardly change in the orthogonal direction of the tool offset (near receiver 10 and receiver 28, approximately 90° and 270°). The amplitude of the collar wave is very sensitive to the direction of tool eccentricity.

The effects of the tool eccentricity on the P-wave arrival times are not obvious, and the main changes in the P-waves are still reflected in their amplitudes. The amplitude of the P-wave increases with increasing eccentricity, and there is increasing interference between
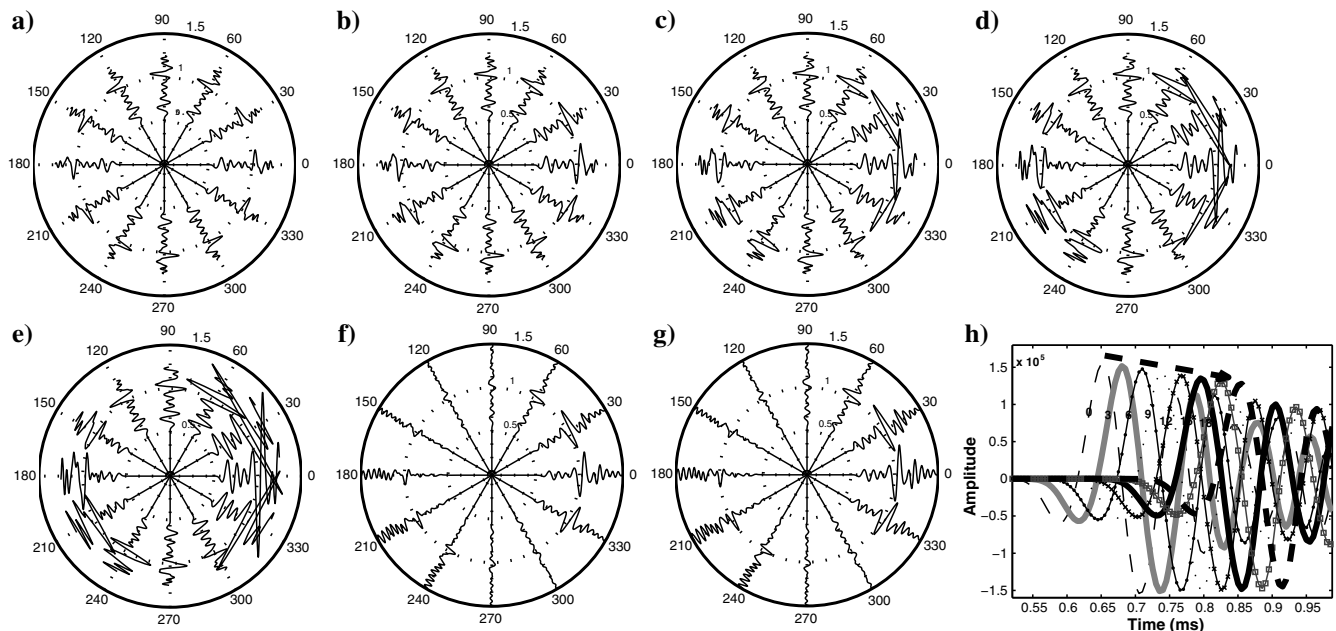

Figure 3. Collar and P-waves in the fast formation for receivers at different azimuths for different tool eccentricities displayed using polar coordinates. The circumference of the coordinates is the angle of the azimuth receiver to receiver 1, and the radial direction is time. Time goes from 0 to 1.5 ms. Panels (a-g) are the waveforms for tool offsets of 0, 3, 6, 9, 12, 15, and 18 mm, respectively. The same maximum-amplitude scale is used for all the waveforms except that panels (f and g) are minified five times. (h) The collar waves at receiver 19 (azimuth of 180°) for different tool offsets.
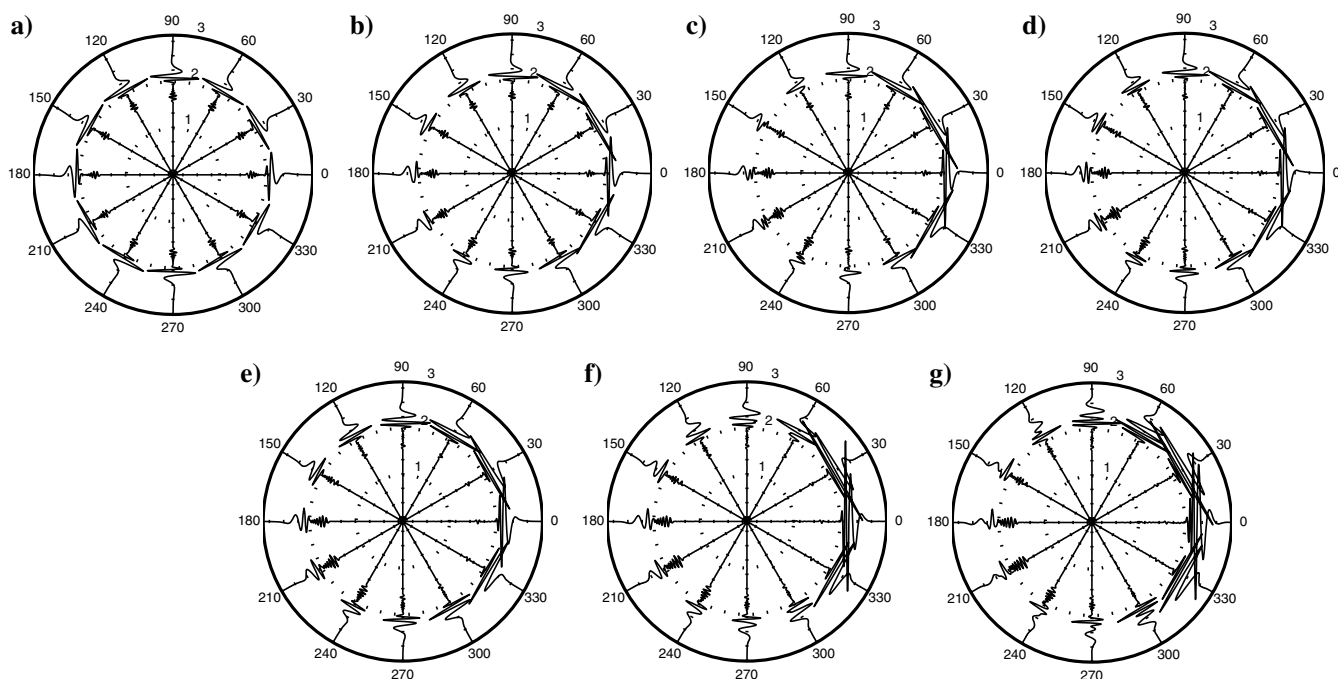
Figure 4. Waveforms for 0 to 3 ms in the fast formation for receivers as shown in Figure 3. Waveforms for tool offsets of (a) 0, (b) 3, (c) 6, (d) 9, (e) 12, (f) 15, and (g) 18 mm. The same maximum-amplitude scale is used for all waveforms.
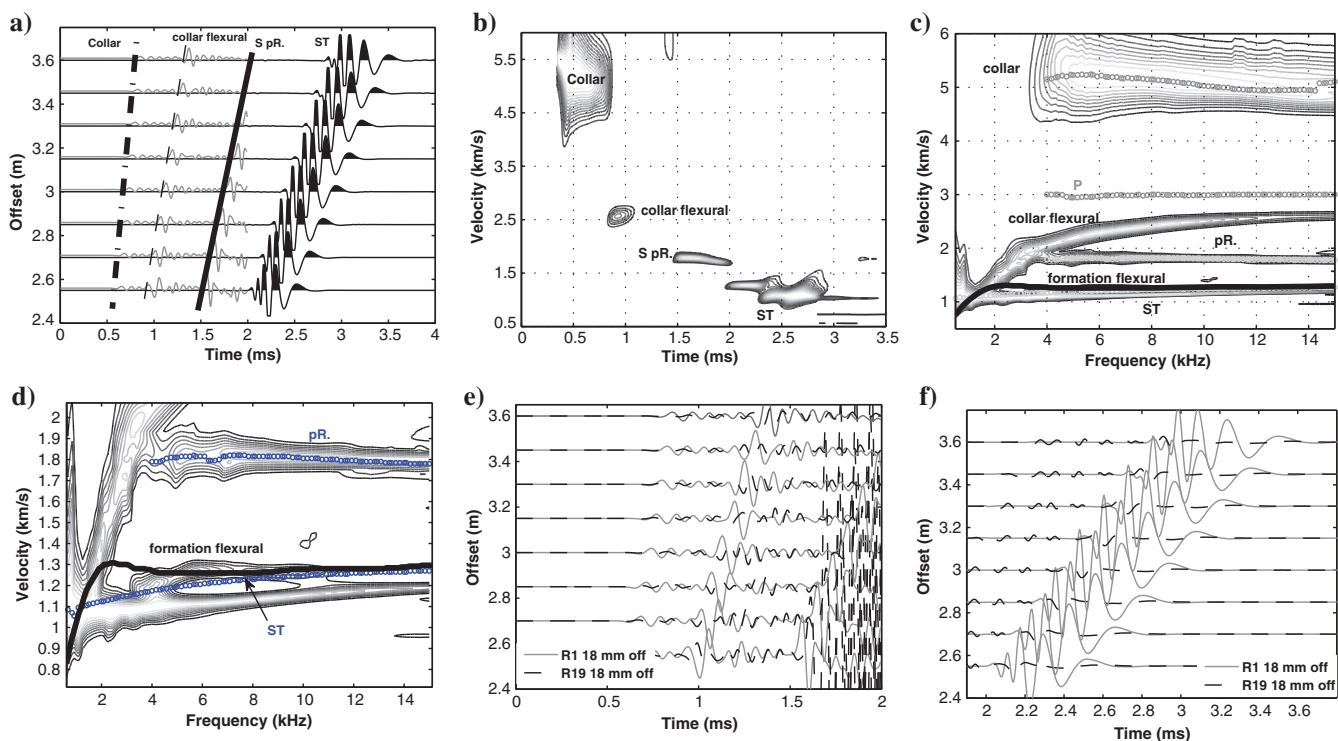

Figure 5. (a) Waveforms in the fast formation, (b) velocity-time semblance, and (c) dispersion for waves at the azimuth of receiver 1 with a tool eccentricity of 18 mm; the gray circles indicate the expected dispersion for a centralized tool (dispersion of the ST-wave for a centralized tool is marked by a black dotted-dashed line to make the change in the ST-wave for an off-center tool clear). (d) The dispersion of formation flexural and ST modes are shown to illustrate the details. (e) The first 2 ms of waveform at receivers 1 and 19 and (f) the waveform (after 2 ms) in the azimuths of receivers 1 and 19.

the collar and P-waves, especially for the receivers near receiver 1. This interference will make the determination of the velocity of P-wave more difficult, but there is little interference in the orthogonal direction of tool eccentricity.

We also show the entire waveforms for different azimuth receivers in Figure 4 just like we did in Figure 3. The same maximum amplitude scale is used for all the waveforms. We now discuss the characteristics of the S-wave and ST-wave with changes in tool eccentricity. From Figure 4, we clearly find that the waveforms near the direction of tool offset change significantly. The amplitude of the ST-wave (approximately 2 ms) in the direction of the minimum

fluid column increases with the tool offset, and this affects the S-wave to some extent (approximately 1.5 ms). However, the amplitude of the ST-wave near receiver 19 becomes smaller as the tool offset increases.

Figure 5 shows the array waveforms, velocity-time semblance, and dispersion for data recorded on receivers with azimuth of 0° (receiver 1) with a tool offset of 18 mm. We find that the amplitudes during the first 2 ms of the waveforms are very low and the collar wave can only be seen after zooming in. We cannot find any information about the P-wave (approximately 3000 m/s in Figure 2b) from the velocity-time semblance (Figure 2b). However, the veloc-
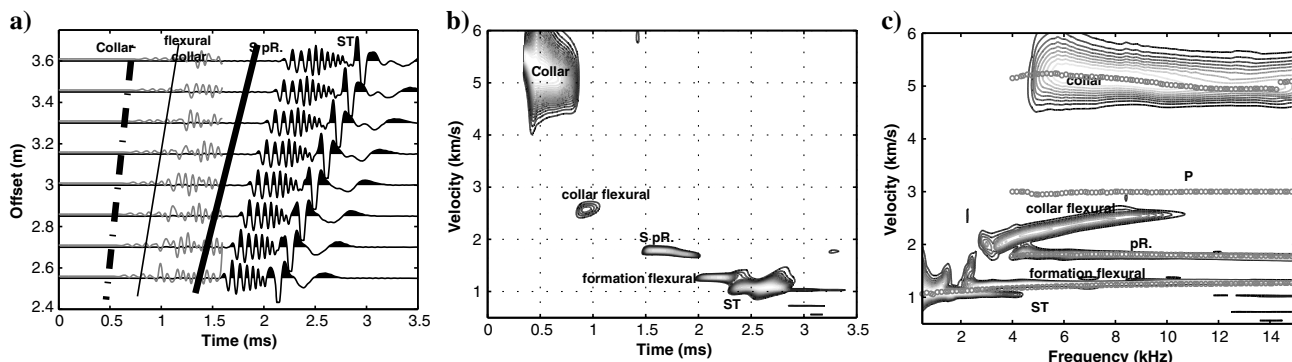

Figure 6. (a) The waveform in the fast formation, (b) velocity-time semblance, and (c) the dispersion in azimuth of receiver 19 with a tool offset of 18 mm.
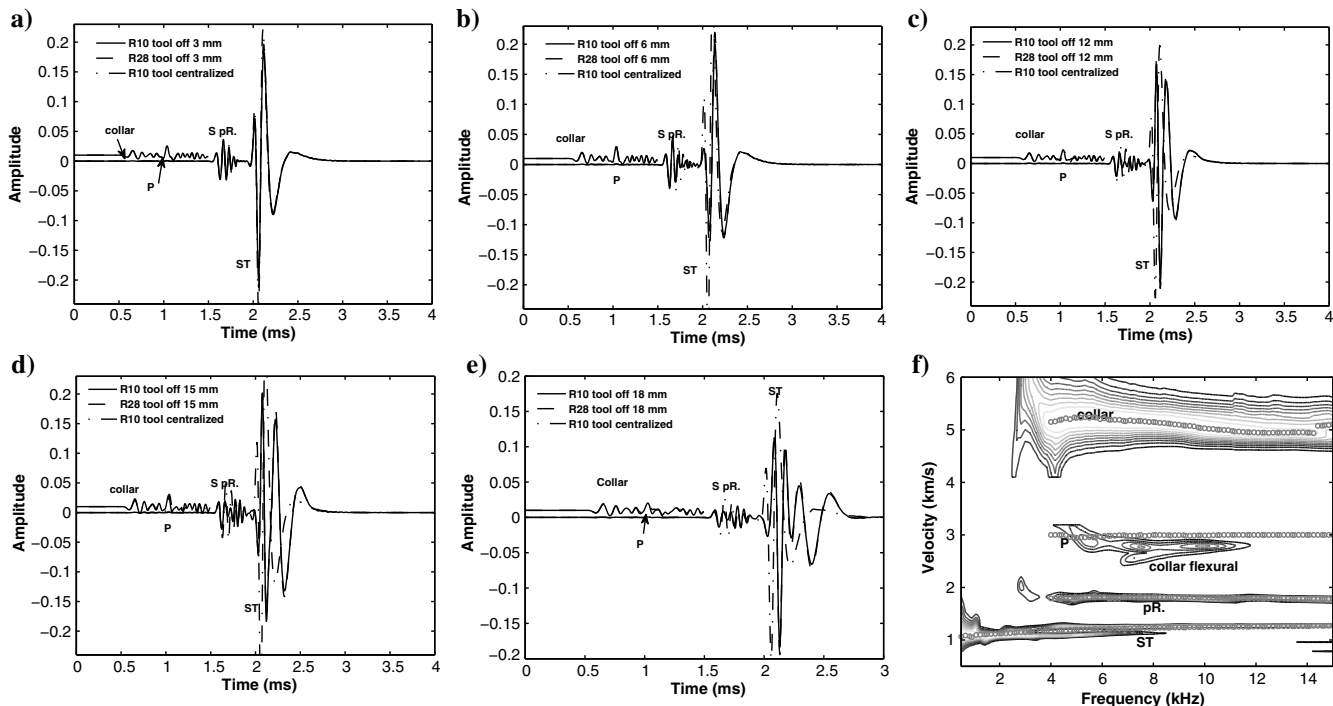

Figure 7. Waveforms in the fast formation for receivers 10 and 28 for different tool offsets. Lines labeled R10 tool centralized, R10 tool off 18 mm, and R28 tool off 18 mm are receiver 10 of a centralized tool, receivers 10 and 28 for the tool offset of 18 mm, respectively. Waveforms for tool eccentricities of (a) 3, (b) 6, (c) 12, (d) 15, and (e) 18 mm. (f) The dispersion analysis for the waveform at the azimuth of receiver 10 with a tool offset of 18 mm (the white circles are the dispersion for the centralized tool case).

ity-time semblance shows an arrival having good coherence at around (1 ms, 2500 m/s), which propagates at a velocity between those of the P- and S-waves. The information about the S-wave is very clear. However, the two good coherence arrivals after 2 ms make the velocity of the ST-wave difficult to discern. The dispersion calculated from the waveforms is shown in Figure 5c, and the dispersion curves calculated from FDM array waveforms calculated for a centralized tool are marked by gray circles for a reference (dispersions of formation flexural mode for a centralized dipole tool is marked by the black solid line). The dispersion curves of formation flexural and ST modes are shown in Figure 5d to illustrate the details. We can easily see a good agreement with the dispersion of the collar wave, pR wave for the centralized tool. Dispersion of the P-wave cannot be identified. In addition, the dispersion curves of the collar flexural and formation flexural waves can be obviously seen in Figure 5c and 5d. To highlight the collar wave, we show the first 2 ms of waveforms as a function of offset along the azimuths of receivers 1 and 19 in Figure 5e. One can easily see the opposite phases of the flexural collar waves (approximately 1.0 ms) between the two azimuths. This change in phase is a clear characteristic of the flexural collar wave between the collar wave and S-wave. It corresponds to the good coherence area around (1 ms, 2500 m/s) in Figure 5b.

We consider that the collar wave for the off-center monopole tool consists of a superposition of the collar monopole wave, the collar flexural wave, and other modes, which will make it more difficult to determine the P-wave velocity than when the tool is centralized. The errors in the determination of the P-wave velocity using waves in the direction of receiver 1 are 21.67%, 20%, 18.67%, 18%, 17.67%, and 17.17% for tool eccentricities of 3, 6, 9, 12, 15, and 18 mm,

respectively. Errors for measurement using receiver 19 are 9%, 13.83%, 14.67%, 15%, 14.67%, and 14.33% for tool eccentricities of 3, 6, 9, 12, 15, and 18 mm, respectively. Comparison of waveforms in Figure 5a with the waveforms for the centralized tool case (after 2 ms in Figure 2a) leads us to expect that the waveform after 2 ms in Figure 5a should be the ST-wave. However, the ST-waves for the cases of offset tools suffer from interference with many other modes and are too complicated to be unraveled. The complexity of the waves arriving at the expected time of the ST-waves is reflected in two obvious regions of high amplitude after 2 ms in the semblance plot shown in Figure 5b. The amplitudes of the initial portion of the ST-waves in the directions of receivers 1 and 19 do not change with offset, whereas the polarities in the two receiver directions are opposite as seen in Figure 5f, which illustrates the formation flexural wave in front of the ST wave. We can examine the detail of the dispersion of the ST wave in Figure 5d. The ST wave becomes slightly slower than for the centralized tool case. The formation flexural wave appears with a velocity that is slightly higher than the ST wave, which can help us to discern the two high-semblance regions after 2 ms in Figure 5b. The region with higher velocity is the formation flexural wave and that with a lower velocity is the ST-wave.

In the same way as in Figure 5, we show in Figure 6 the waveforms versus offset, velocity-time semblance, and the dispersion at the azimuth of receiver 19 for a tool offset of 18 mm. The collar monopole and flexural waves are obvious from the array waveforms in Figure 6a. We can easily extract the velocities of modes from velocity-time semblance (Figure 6b). The dispersion (Figure 6c) clearly shows the extra flexural collar and formation waves that are not present when the tool is centralized. It follows that the
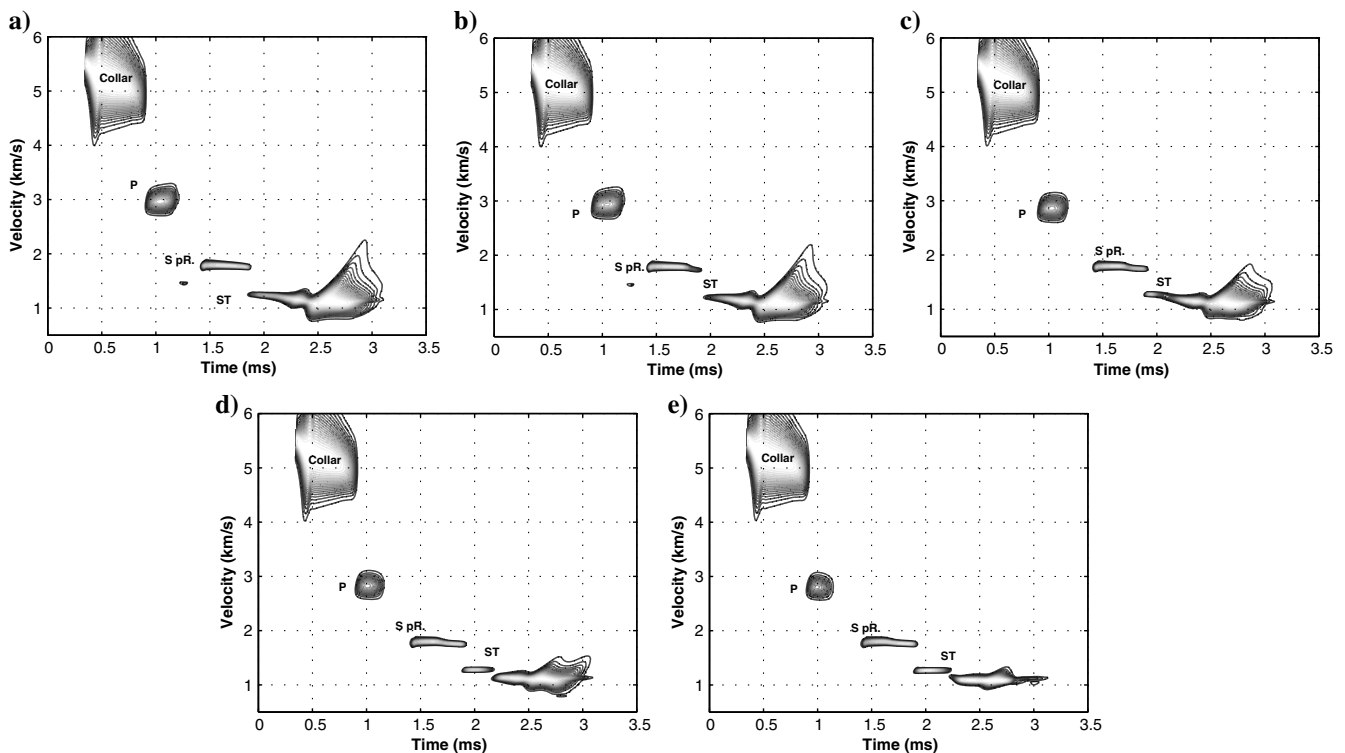

Figure 8. Velocity-time semblances for the waveform in the fast formation for azimuth of receiver 10 for different tool offsets: (a) 3, (b) 6, (c) 12, (d) 15, and (e) 18 mm.

collar flexural modes and other higher modes will appear with increasing tool eccentricity. The S-wave can be seen on the waveform in the off-center tool case. The multimode collar wave makes the identification of the P-wave difficult. We can see that the last wave packet of the ST-wave consists of several modes (Figure 6a),

including the flexural wave in front of the ST-wave and the low-frequency wave at the end of the ST-wave (approximately 2.5 ms), which corresponds to the coherent phase with the latest arrival time and the lowest velocity (2.5 ms, 1050 m/s). The interference of the various modes is reflected in the dispersion curves of the
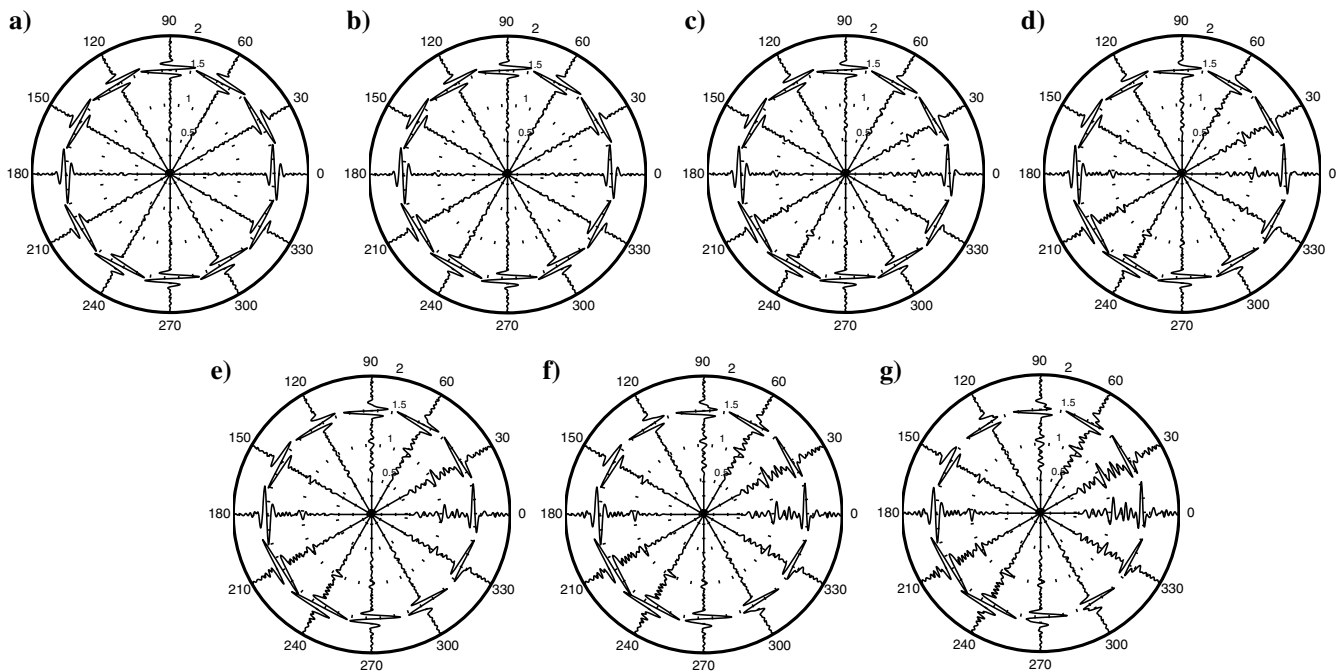

Figure 9. Polar coordinate plots of the collar and P-waves in the slow formation for receivers at different azimuths for different tool offsets. Plot organization is the same as that in Figure 3. Thee time range is from 0 to 2 ms. Tool offsets of (a) 0, (b) 3, (c) 6, (d) 9, (e) 12, (f) 15, and (g) 18 mm are shown. The same maximum-amplitude scale is used for all of the waveforms.
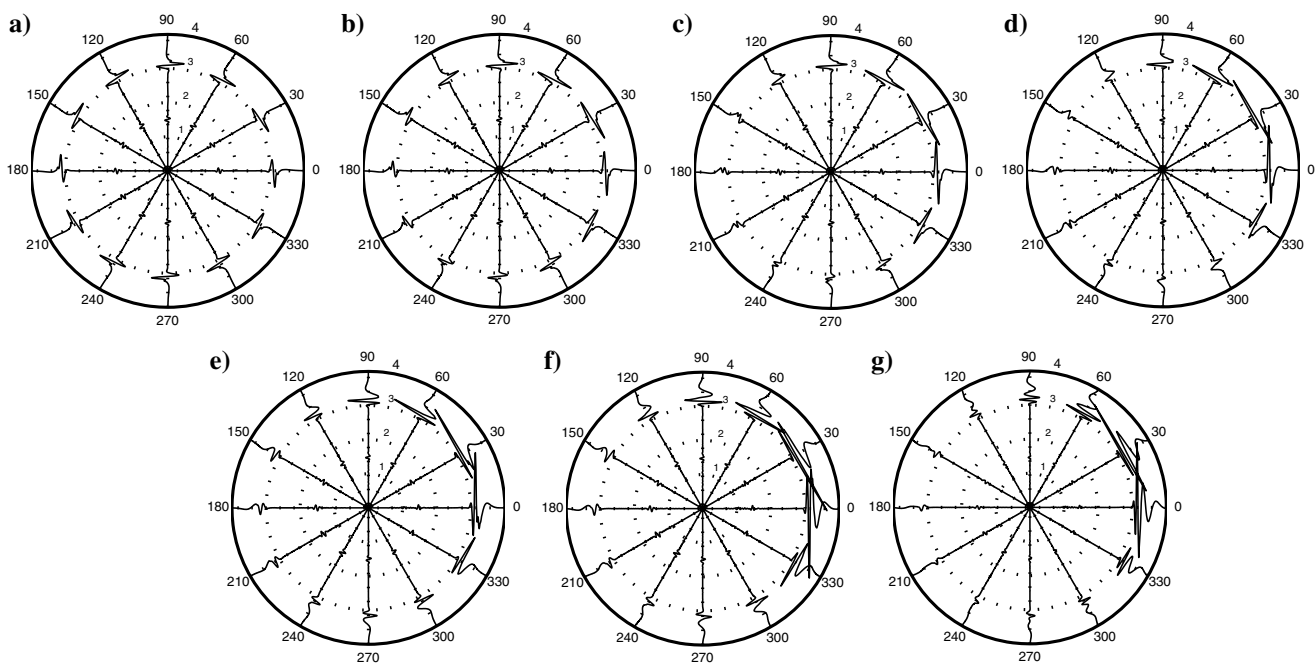

Figure 10. Waveforms from 0 to 4 ms in the slow formation for receivers at different azimuths with different tool offsets. Waveforms for tool offsets of (a) 0, (b) 3, (c) 6, (d) 9, (e) 12, (f) 15, and (g) 18 mm. The same maximum-amplitude scale is used for all of the waveforms.

formation flexural and ST-waves (Figure 6c). The ST-wave becomes slower than in the centralized tool case, and the velocity of the formation flexural wave is slightly higher than that of the ST-wave.

For the receivers in the direction orthogonal to the tool offset, the tool eccentricity does not affect the waveforms severely. In Figure 7, we plot the waveforms for receivers 10 and 28 for different tool offsets. Lines labeled R10 tool centralized, R10 tool off 18 mm, and R28 tool off 18 mm are for receiver 10 of a centralized tool and for receivers 10 and 28 for a tool offset of 18 mm, respectively. Figure 7 is the waveforms for tool offsets of 3, 6, 12, 15, and 18 mm. On the whole, the waveforms at receivers 10 and 28 do not change much with tool eccentricity. The waveforms are hardly affected with the tool eccentricity of 3 and 6 mm, with only the amplitude of ST-wave reduced a little. However, other phases change little with only a slight change in the P-wave in receivers 10 and 28 when a tool offset is 12 mm. The polarity difference between the waveforms at two receivers is not obvious even for tool offsets of 15 and 18 mm.

The determination of the P-wave velocity will not be severely affected by the weak collar flexural wave at receivers 10 and 28 when the tool is off center. We do find some changes in the dispersion curves for off-center tools compared to centralized tools. Figure 7f shows the results of dispersion analysis for the waveform at receiver 10 with a tool offset of 18 mm. Gray circles denote the dispersion curves for a centralized tool as a reference. It can be seen that the P-wave becomes a little more dispersive compared to the case of a centralized tool, and it is also slightly influenced by the collar flexural wave. However, these will not cause a big problem for identification of the P-wave. Two modes appear in the ST-wave, and their amplitudes increase with the tool offset. The fast mode (appears above the ST dispersion curve for the tool centralized case) is the formation flexural mode, and the slow mode (appears below the curve of ST wave in centralized case) is the ST mode in this case (as shown in Figure 7f).

Figure 8 shows the velocity-time semblance for waveforms at receivers along the azimuth of receiver 10 for tool eccentricities of 3, 6, 12, 15, and 18 mm. The peak values of velocity-time
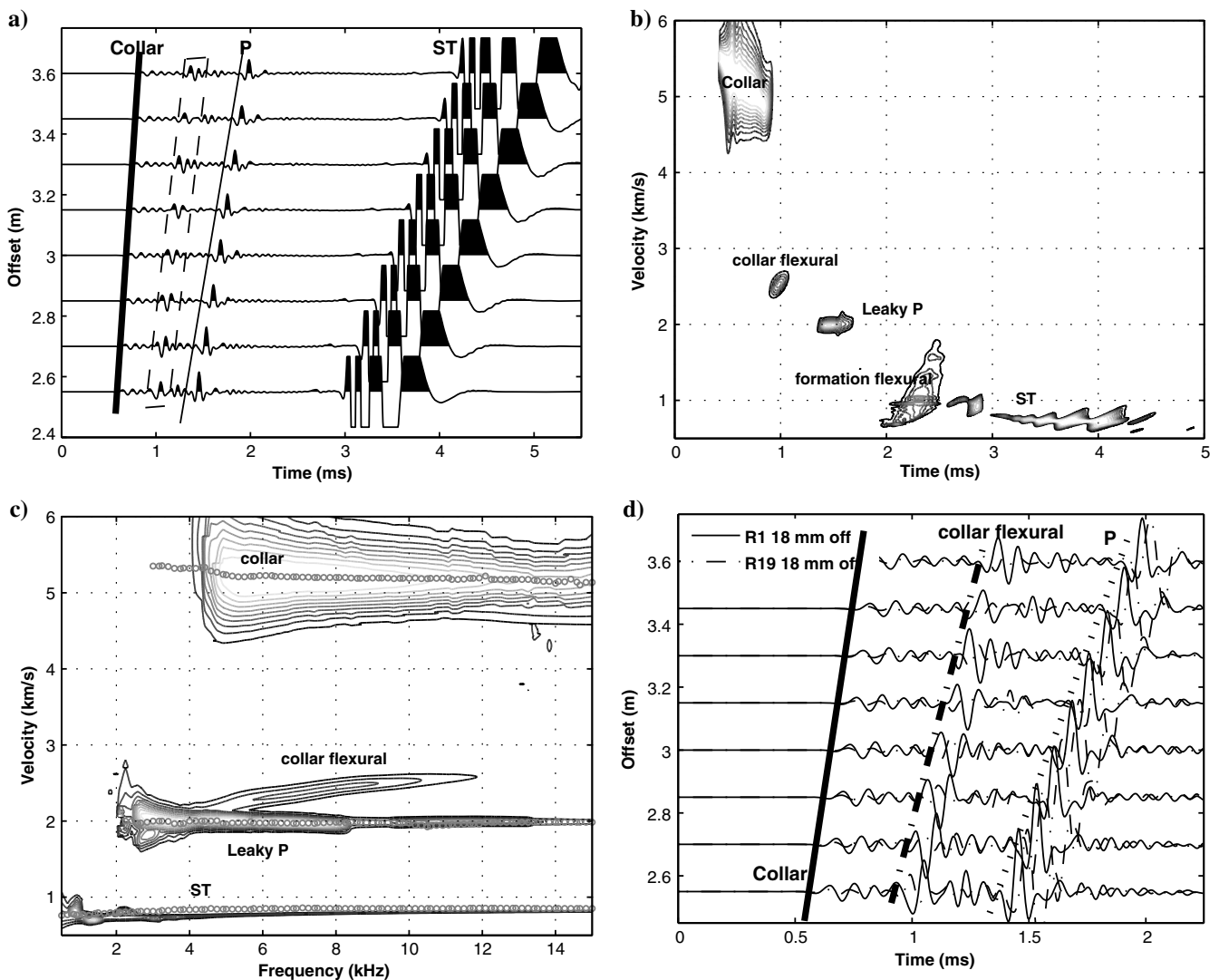

Figure 11. (a) Array waveforms for the slow formation, (b) velocity-time semblance plot, and (c) the dispersion analysis for the waveform in the azimuth of receiver 1 with the tool offset of 18 mm. (d) The first 2 ms of the waveforms in the azimuths of receivers 1 and 19.

Wang et al.

semblance plots are 2960, 2935, 2860, 2825, and 2800 m/s for Figure 8a–8e, respectively. The errors in the determination of P-wave velocities for receivers along the azimuth of 10 for tool off-centers of 3, 6, 12, 15, and 18 mm are 1.33%, 2.17%, 4.67%, 5.83%, and 6.67%, respectively. The trend of decreasing velocity of the apparent P-wave with increasing tool eccentricity results from interference with the collar flexural wave.

We now briefly summarize the influence of tool eccentricity on the high-frequency (around 10 kHz) monopole data in a fast formation:

1) The P-wave velocity can be determined directly for a centralized tool when the velocity difference between the collar and formation is large. However, if the velocity difference is not large, the P-wave may be influenced by the collar wave and special means such as tool grooves (e.g., Leggett et al., 2001; Kinoshita et al., 2010) should be adopted to eliminate the interference.
2) More collar modes, including monopole, dipole, and even quadrupole modes, appear on receivers in the direction of the tool offset. Their amplitudes increase with the increasing tool offset,

which makes the identification of the P-wave more difficult than in the centralized tool case. The effects are not severe in the orthogonal direction of the tool offset.
3) The tool offsets have minimal effect on the determination of the S-wave velocity.
4) The ST-wave from an off-center tool is slightly slower than the one for a centralized tool.

THE RESPONSE OF THE ECCENTRIC ACOUSTIC MONOPOLE LOGGING-WHILE-DRILLING TOOL IN A SLOW FORMATION

We will now look at the effects of tool eccentricity on mode waves (the collar and P-waves) in a slow formation. Figure 9 shows the waveforms in different azimuths for the tool offsets of 0, 3, 6, 9, 12, 15, and 18 mm. The same maximum-amplitude scale is used for all of the waveforms. It is obvious that the tool being off center does not affect the arrival time of the collar wave (approximately 1 ms) compared to arrival times for a centered tool. The amplitude of the
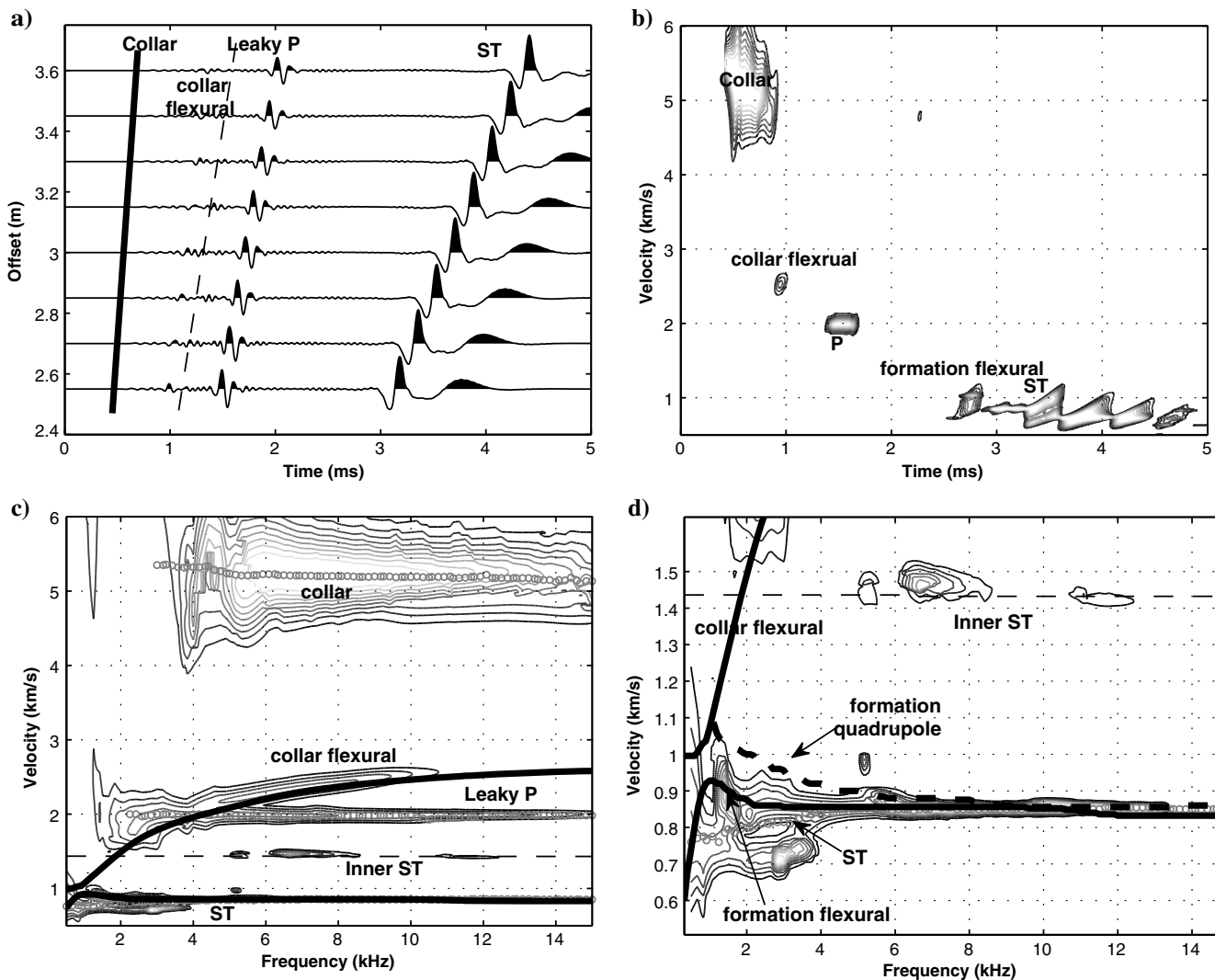

Figure 12. (a) Array waveforms for the slow formation, (b) velocity-time semblance plot, (c) the dispersion analysis for the waveforms in the azimuth of receiver 19 for the tool offset of 18 mm, and (d) dispersion curves showing only velocities less than 1500 m/s.

collar wave increases with increasing tool offset for the receivers in the direction of the tool eccentricity. However, the amplitude of the collar waves for receivers located orthogonal to the directions of the tool eccentricity are not severely affected.

The interference from the collar wave may cause difficulties for determination of the P-wave velocity for receivers at 0° and 180° relative to the tool offset direction. The interference is not significant to the P-wave at receivers near 180°, as shown in Figure 9b–9g. Figure 10 shows the waveforms in the time interval from 0 to 4 ms at different azimuths for tool offsets of 0, 3, 6, 9, 12, 15, and 18 mm. The same maximum-amplitude scale is used for all of the waveforms. It is hard to see the small-amplitude collar waves on the longer duration waveforms. Only the P-wave and ST-wave (approximately 3 ms) can be clearly identified. The amplitudes of the ST-waves (3 ms) in the direction of the smallest and largest fluid columns exhibit different effects due to the tool eccentricity. The latter one decreases with the increasing tool offset. However, the former increases with the tool offset.

We now analyze the array waveforms in the directions of receivers 1, 10, and 19 with a tool offset of 18 mm. Figure 11 shows the array waveforms, velocity-time semblance plot, and the dispersion analysis for waveforms in the direction of receiver 1. We can identify the collar, P-, and ST-waves clearly in the array waveforms shown in Figure 11a. The increase in amplitude of the ST-wave caused by an off-center tool makes the amplitudes of the collar and P-waves look smaller, although they are almost the same as those in the centralized tool case. A new signal appears between the collar wave and the P-wave in the region between the dashed lines in Figure 11a. Such a signal may cause problems for the determination of P-wave velocity. We can find the coherence of the signal in the velocity-time semblance plot (as shown in Figure 11b).

From the dispersion analysis shown in Figure 11c, the new signal can be identified as a collar flexural wave that is not present in the centralized tool case (marked by gray circles). The first 2 ms of the waveforms at receivers 1 and 19 are shown in Figure 11d. The po-
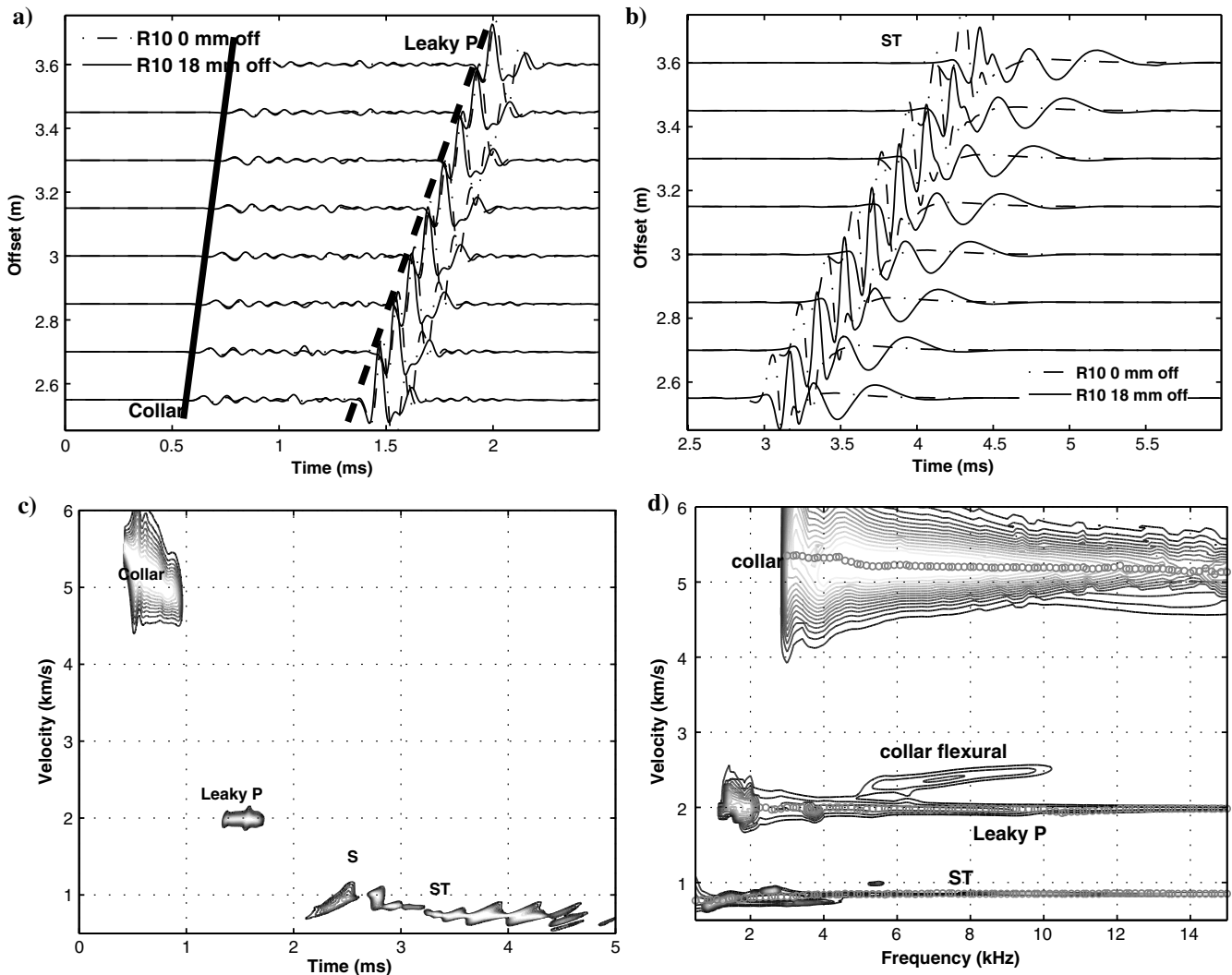

Figure 13. (a) Array waveforms in the slow formation of the collar wave and leaky P-waves, (b) array waveforms of the ST wave, (c) velocity-time semblance plot, and (d) the dispersion analysis for the waveform in the azimuth of receiver 10 for the tool eccentricity of 18 mm.

larity difference of the collar flexural waveforms at the two receivers can be clearly seen. Experience with dipole sources tells us that the strong collar flexural mode should be accompanied by a formation flexural mode (Wang and Tao, 2011) that arrives after the P-wave. Although this is not seen here due to the huge amplitude of the ST-waves, we can still find interference of the formation flexural wave on the ST-wave below 2 kHz (Figure 11c). Moreover, small differences can be found between the dispersion of the ST-wave for the offset tool and the centralized tool case: The velocities for some frequencies are lower than that of the centralized tool case (gray circles). Figure 12 shows information about array waveforms in the azimuth of receiver 19 with a tool offset of 18 mm. Figure 12a shows that the interference between the collar and leaky P-waves is not as severe as that found at receiver 1 (Figure 11a). However, the dispersion characteristics of the collar flexural wave shown in Figure 12c show that the wave clearly does severely disturb the leaky P-wave in the low-frequency band below 4 kHz. The collar flexural wave makes determination of the P-wave velocity a bit difficult, as it is usually obtained from dispersion of the leaky P-wave (e.g., Wang and Tao, 2011). Therefore, a good dispersion analysis method is needed. The errors in determination of the P-wave velocities for different tool eccentricities are around 1.25%, which are not bad. The collar flexural mode also perturbs the ST mode at very low frequencies (less than 1 kHz in Figure 12c). The waveforms around 3 ms look complicated, and the low-frequency component is very different from that in the ST in the tool centralized case. From the velocity-time semblance plot in Figure 12b, we can also find multiple high-semblance regions after 3 ms. To understand the modes existing in the waveforms, we plot dispersion curves for the centralized monopole and dipole tools in Figure 12c and give an expanded view for velocities less than 1500 m/s in Figure 12d. We can see the characteristics of the inner ST-wave (the ST-wave that propagates along the inner collar surface) with a velocity of approximately 1400 m/s, the quadrupole and formation flexural waves, and the ST-wave (near the velocity of 1000 m/s) in the dispersion plot. The new modes identified are flexural and quadrupole waves, and the waveforms after 3 ms in Figure 12a consist of a combination of the inner ST-wave, ST-wave, flexural wave, and even the quadrupole wave.

Figure 13 shows the waveforms in the azimuth of receiver 10 for the centralized tool and for one with an offset of 18 mm. Figure 13a shows the portion of the collar and leaky P-wave, and Figure 13b shows the ST-wave. Dashed and solid lines are for waveforms for the centralized tool and a tool with an offset of 18 mm, respectively. We can see very little difference between the collar waves for the two tool positions. The subtle differences result from the strong collar flexural wave and weak collar quadrupole wave indicated by dispersion analysis (as shown in Figure 13d). We find that the tool offset does not affect the collar wave for receiver 10. For the leaky P-wave, the tool offset lowers the amplitude a little. The ST waveform is affected by the tool offset mostly in two ways (as shown in Figure 13b): (1) the delay of the arrivals and (2) the generation of other modes. From dispersion analysis (Figure 13d), we find that the part of waveforms consist of the ST, flexural and quadrupole modes, which have velocity of approximately 1000 m/s and frequency less than 4 kHz.

We conclude that for the off-center tool in the slow formation, although the collar flexural mode appears on the receivers in the direction of tool eccentricity, it does not severely affect the determination of the P-wave velocity. A good dispersion analysis method

helps us to reduce the interference of collar flexural wave on leaky P-wave in the low-frequency band (less than 4 kHz). The off-center tool affects the ST-wave in many ways and brings out more weak formation modes.

CONCLUSIONS

We have applied the FDM to simulate the response of a noncentralized monopole high-frequency (10 kHz) ALWD tool in fast and slow formations. Based on the simulation results, we analyzed the influence that tool offsets have on the waveforms from receivers at different azimuths. Our conclusions are as follows:

1) The off-center tool changes waveforms. The waveform in the direction of the tool offset is affected severely, with the waveforms near the smallest fluid column being affected the most. However, the waveform in the orthogonal direction of the tool offset is hardly affected by tool eccentricity.
2) Obvious collar flexural and collar quadrupole waves appear when the tool is off-center. New modes such as the formation flexural and formation quadrupole waves appear before and during the ST wave.
3) The tool offset affects the waveforms in fast and slow formations in different ways. Waveforms in a fast formation are more seriously affected by the tool offsets, and the new collar modes hinder the determination of the P-wave velocity in the direction of tool offset. The determination of the P-wave velocity in the orthogonal direction is easier than in the direction of tool offset. However, the new collar modes do not significantly affect the determination of the P-wave velocity in a slow formation.

Given the complexity of how waveforms are influenced by a tool being off-center, we consider that a simple superposition of all the waveforms for receivers at different azimuths for an off-center monopole tool will not provide reliable assessments of elastic formation properties. When making an ALWD measurement, one should first quantify the tool eccentricity by an off-center dipole measurement at the same time and then use a suitable data correction method to avoid the effects of tool eccentricity. Based on the corrected data, the conventional acoustic logging data processing method such as velocity-time semblance method could be used to obtain the velocities of the P- and S-waves.

ACKNOWLEDGMENTS

REFERENCES

Dziewonski, A., S. Block, and M. Landisman, 1969, A technique for the analysis of transient seismic signals: Bulletin of the Seismological Society of America, **59**, 427–444.
Huang, X., 2003, Effects of tool positions on borehole acoustic measurements: A stretched grid finite difference approach: Ph.D. thesis, MIT.
Huang, X., Y. Zheng, and M. N. Toksoz, 2004, Effects of tool eccentricity on acoustic logging while drilling (LWD) measurements: 74th Annual International Meeting, SEG, Expanded Abstracts, 290–293.

Kimball, C. V., and T. Marzetta, 1984, Semblance processing of borehole acoustic array data: Geophysics, **49**, 274–281, doi: 10.1190/1.1441659.

Kinoshita, T., A. Dumont, H. Hori, N. Sakiyama, J. Morley, and F. Garcia-Osuna, 2010, LWD sonic tool design for high-quality logs: 80th Annual International Meeting, SEG, Expanded Abstracts, 513–517.

Leggett, J. V., V. Dubinsky, D. Patterson, and A. Bolshakov, 2001, Field test results demonstrating improved real-time data quality in an advanced LWD acoustic system: Presented at SPE Annual Technical Conference and Exhibition, 71732.

Moore, J., V. Dubinsky, C. Harrison, and C. Li, 2008, LWD acoustic measurements enhancements for varying drilling conditions: Presented at Europec/EAGE Conference and Exhibition, 113486.

Pardo, D., P. J. Matuszyk, I. Muga, C. Torres-Verdín, A. Mora, and V. M. Calo, 2013, Influence of borehole-eccentered tools in wireline and LWD sonic logging measurements: Geophysical Prospecting, **61**, 268–283, doi: 10.1111/1365-2478.12022.

Rao, Rama, V. N., and Toksoz, M. Nafi, 2005, Dispersive wave analysis — Method and applications: Earth Resources Laboratory Industry Consortia, Annual Report, 2005–04.

Tang, X. M., and C. H. Cheng, 2004, Quantitative borehole acoustic methods: Elsevier Science Publishing Company, Inc.

Tang, X. M., D. Patterson, V. Dubinsky, C. W. Harrison, and A. Bolshakov, 2003, Logging-while-drilling shear and compressional measurements in varying environments: SPWLA 44th Annual Logging Symposium, paper II.

Tang, X. M., D. Patterson, D. Patterson, and L. Wu, 2009, Measurement of formation permeability using Stoneley waves from an LWD acoustic tool: Presented at SPWLA 50th Annual Logging Symposium, paper v51n2a1.

Tang, X. M., Y. Zheng, and D. Vladimir, 2004, Logging while drilling acoustic measurement in unconsolidated slow formations: Presented at SPWLA 46th Annual Logging Symposium, paper R.

Wang, H., and G. Tao, 2011, Wavefield simulation and data-acquisition-scheme analysis for LWD acoustic tools in very slow formations: Geophysics, **76**, no. 3, E59–E68, doi: 10.1190/1.3552929.

Wang, H., G. Tao, and K. Zhang, 2013a, Wavefield simulation and analysis with the finite-element method for acoustic logging while drilling in horizontal and deviated wells: Geophysics, **78**, no. 6, D525–D543, doi: 10.1190/geo2012-0542.1.

Wang, H., G. Tao, X. Shang, X. Fang, and D. Burns, 2013b, Stability of finite difference numerical simulations of acoustic logging-while-drilling with different perfectly matched layer schemes: Applied Geophysics, **10**, 384–396, doi: 10.1007/s11770-013-0400-6.

Wang, H., G. Tao, and X. Zhang, 2009a, Review on the development of acoustic logging while drilling (in Chinese with English abstract): Well Logging Technology , **33**, 197–203.

Wang, H., G. Tao, B. Wang, W. Li, and X. Zhang, 2009b, Wavefield simulation and data acquisition scheme analysis for LWD acoustic tool (in Chinese): Chinese Journal of Geophysics, **52**, 2402–2409.

Wang, T., and X. Tang, 2003, Investigation of LWD quadrupole S measurement in real environments: Presented at SPWLA 44th Annual Logging Symposium, paper KK.

Zhan, X., Z. Zhu, S. Chi, and M. Toksöz, 2010, Elimination of LWD (logging while drilling) tool modes using seismoelectric data: Communications in Computational Physics, **7**, 47–63, doi: 10.4208/cicp.2009.08.174.

Zheng, Y., X. Huang, and M. N. Toksoz, 2004, A finite element analysis of the effects of tool eccentricity on wave dispersion properties in borehole acoustic logging while drilling: 74th Annual International Meeting, SEG, Expanded Abstracts, 294–297.